

PHASE SHIFT-DIGITAL SPECKLE PATTERN INTERFEROMETRY AND OPTIMIZATION FOR BONES DISPLACEMENTS PREDICTION

Rolando J. González-Peña

Universitat de València. Departamento de Fisiología, Facultad de Medicina y Odontología, Valencia, Spain

E-mail: rolando.j.gonzalez@uv.es

Ricardo Rodrigues Magalhaes

Universidade Federal de Lavras/UFLA, Departamento de Engenharia/DEG, Lavras, MG, Brazil

Corresponding author: E-mail: ricardorm@deg.ufla.br

Roberto Alves Braga Junior

Universidade Federal de Lavras/UFLA, Departamento de Engenharia/DEG, Lavras, MG, Brazil

E-mail: robbraga@deg.ufla.br

Danton Diego Ferreira

Universidade Federal de Lavras/UFLA, Departamento de Engenharia/DEG, Lavras, MG, Brazil

E-mail: danton@deg.ufla.br

Abstract: The use of phase shift-digital speckle pattern interferometry (DSPI) together with an optimization method for displacement prediction of a bone sample was evaluated. The proposed method is based on Particle-swarm Optimization (PSO) algorithm which used analytical data to obtain the bone Young's modulus for Finite Element Analysis (FEA) simulations in order to compare with experimental displacements results from DSPI. A bone sample was used in the experiments for generating the displacements by using DSPI, PSO algorithm identified the optimized Young's modulus and FEA was used to simulate displacements from the bone geometry model. Results presented good agreement between FEA and DSPI data showing error around 3%. This can be considered a potentiality of DSPI supported by optimization method and FEA for displacement prediction in bone samples.

Keywords: Particle-swarm optimization; Bone sample; Displacement measurements.

Received: May, 12 2016 - Accepted: January, 13 2017

INTRODUCTION

Digital Speckle Pattern Interferometry (DSPI) is a technique commonly used for micro displacement measurements in structural elements (Facchini and Zanetta (1995); González et al. (2001) and Goodman (2007)). Also, in medicine and in biomedicine fields, applications of DSPI technique are presented (Lang et al. (2004) and Román et al. (1999)) demonstrating the wide range of applications for physics properties that require sensitive approaches to access them properly.

Many investigations on the mechanical properties of bone tissue have reported different values for the modulus of elasticity (Reilly, Burstein and Frankel (1974)). The application of DSPI to determine the elastic characteristics of a bone allows

the study of elastic behavior of these materials in different kind of experiments. Some related works show results for bones measurements by using optics techniques (Martinez-Celorio et al. (2010), Petzing et al. (1998) and Su et al. (2005)).

Since the biological material bring with them an intrinsic variability and heterogeneity, the outputs from the DSPI measurements require a post-processing step for adjusting results to adopt a reliable information. One post-processing approach that can be used in those cases is the particle-swarm optimization (PSO) which is based on socio-psychological principles inspired by swarm intelligence. PSO has been applied in different areas (Arumugam and Rao (2008); Jiang et al. (2007); Liu, Liu and Cartes (2008); Magalhaes, Braga Jr and Barbosa (2015); Mazhoud et al. (2013)

and Loja (2014)), including biomechanics (Hill and Banks (2014); Koh et al. (2006); Koh et al. (2009); Schutte (2005) and Yang et al. (2011)).

Therefore, this work assumed that the adoption of a PSO post-processing of the images from the DSPI application in bones displacements could improve the quality of the outcomes.

This paper is focused on applying DSPI supported by an optimization method in order to predict displacements in a bone sample by using Finite Element Analysis (FEA) (Parvitte et al. (2013)). In this case, the material property is represented by the Young's modulus in order to evaluate the use of DSPI together with optimization for displacements prediction in a bone sample.

Measurement of out of plane displacements by DSPI

Figure 1 presents DSPI components scheme for displacement measurements in the normal direction to the surface of the object. It uses a single He-Ne laser beam which is divided by a beam splitter with a semitransparent mirror with one of the two beams expanded and projected directly to the front surface of the object and reflected through a lens to produce the image in the CCD (Charge Coupled Device) camera. The other beam is the reference one which interferes with the object beam before reach the CCD camera by using a beam combiner cube. Finally, CCD camera records the interference of them and two images are recorded before and after applying the load (P).

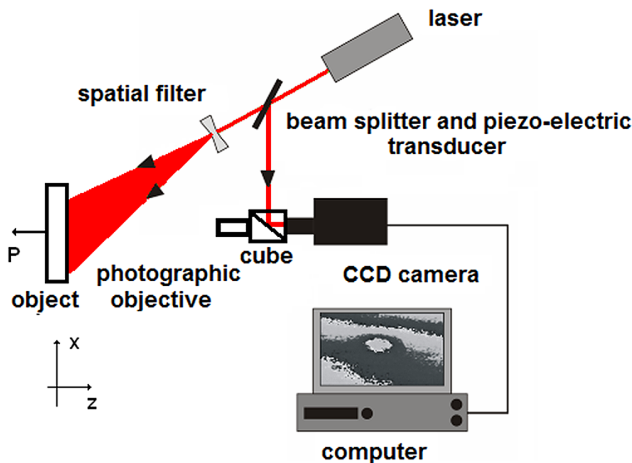


Figure 1: DSPI components scheme for displacement measurements.

Initially a reference image corresponding to the initial stage of the object without applied load is considered. Different images are successively subtracting from the reference image, resulting in a striped box. Given considerations of classical interferometry, the resulting irradiance at a point (x, y) of the image captured by the CCD camera (reference image) is given by Equation (1).

$$I_1(x, y) = I_r(x, y) + I_o(x, y) + 2|\gamma| \sqrt{I_r(x, y)I_o(x, y)} \cos \Psi(x, y) \quad (1)$$

where $I_r(x, y)$ is the uniform intensity of the reference beam and $I_o(x, y)$ is the intensity of the object beam; $|\gamma|$ is the degree of coherence between the two beams (approximately equal to 1), which is a measure of visibility and $\Psi(x, y)$ is the phase difference between the reference beam and the object beam at point (x, y).

When the object undergoes deformation, the new image captured by the CCD camera presents the irradiance according to Equation (2).

$$I_2(x, y) = I_r(x, y) + I_o(x, y) + 2|\gamma| \sqrt{I_r(x, y)I_o(x, y)} \cos [\Psi(x, y) + \phi(x, y)] \quad (2)$$

where $\phi(x, y)$ is the optical phase difference due to the object deformation, which is the surface where the phase shift is experienced by the speckle pattern.

When the magnitude of the final image is squared, it is obtained successive images subtraction from the reference image which is represented by Equation (3).

$$|I_1(x, y) - I_2(x, y)|^2 = |4I_r(x, y)I_o(x, y)|\gamma|^2 \sin^2 \left[\Psi(x, y) + \frac{\phi(x, y)}{2} \right] \sin^2 \frac{\phi(x, y)}{2} \quad (3)$$

Furthermore, the phase difference is directly related to the optical path difference of the illumination beam from the object, before and after the displacement of the point of interest. The component of the displacement outside the plane $z(x, y)$ is related to the phase difference $\phi(x, y)$ according to Equation (4).

$$d(x, y) = \left[\frac{\lambda}{2\pi(1 + \cos \theta)} \right] \phi(x, y) \quad (4)$$

where $d(x, y)$ is the displacement and θ is the illumination angle.

In order to improve the quality of the final image, a phase-shifting process is carried out where four consecutive pictures from the object are created by adding a displacement of $\pi/2$ between them through a piezoelectric transducer coupled to a side mirror. The phase map has a phase interval between $-\pi$ and π being obtained from the Equation (5).

$$\psi(x, y) = \tan^{-1} \left[\frac{(I_4(x, y) - I_2(x, y))}{(I_1(x, y) - 2I_3(x, y))} \right] \quad (5)$$

Through a process of phase unwrapping, the phase of each point of the object is obtained and thus estimates the displacements at specified points of the object.

Considering a homogeneous, linear and isotropic beam subjected to a bending condition, the vertical displacement at centerline is represented by Timoshenko and Goodier (1970) as in the Equation (6).

$$d(x, y) = \frac{P}{2EI} \left(Lx^2 - \frac{x^3}{3} \right) \quad (6)$$

where P is the load, E is the material Young's Modulus, I is the moment of inertia, L is the beam length and x is the distance between the displacement measurement point and clamping position.

Optimization theory

By knowing experimental displacements, PSO algorithm can be applied in order to describe each particle position from the vector position in the search space from Equation (7).

$$v(t+1) = (wv(t)) + (c_1r_1(p(t) - x(t)) + (c_2r_2 (g(t) - x(t))) \quad (7)$$

where w factor is the inertia weight, $v(t)$ is the particle's velocity at time t , $x(t)$ is the particle's current position at time t , c_1 and c_2 are constants weighting, $p(t)$ is the particle's best position, $g(t)$ vector value is the best known position found by any particle in the swarm and r_1 and r_2 are random numbers in a specific range, that normally vary between 0 and 1 (Marwala (2005)).

By applying Equation (5), the new velocity, $v(t+1)$, is used to compute the new particle's position, $x(t+1)$ as presented in Equation (8).

$$x(t+1) = x(t) + v(t+1) \quad (8)$$

Each particle moving towards the previous position tends to an optimized value.

MATERIAL AND METHODS

Experimental displacements from DSPI

In order to evaluate Young's modulus measurements by DSPI and optimization, one sample of a dried radius bone was used. Mechanical experiments (bending tests) were performed in order to provide DSPI measurements data and define the objective function to be used in the PSO algorithm. In the bending test, the bone was clamped in zero position and a static load (P) of 0.098 N was applied 92 mm far from the clamping as schematically shown in Figure 2.

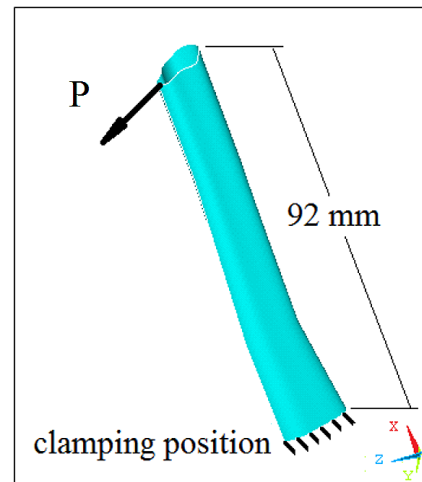


Figure 2: Sample bone drawing and loads position scheme.

Considering the non-regular geometry of the sample, it was necessary to measure the moment of inertia from different positions of the bone. A computed tomography was performed in order to measure the sample thickness at each two millimeters. These points were defined following same positions from the Finite Element model. From the cross sections measurements, a moment of inertia of 468 mm^4 was obtained. For this study, it was not taken into account the trabecular bone tissue because the experiments were provided considering pure bending. If a tensile test from

a tissue is performed, it is necessary to consider the trabecular bone. Although, in long bones such as the femur, this kind of consideration is important.

A He-Ne laser beam with 632.8 nm and 45 mW was used as a source of illumination and after being projected by mirrors and expanded by a spatial filter, the beam reaches the object was illuminated at an angle around 0° . The images were acquired by a macro (SIGMA) with a focal length of 50 mm, iris of $f/16$, connected to an AVT Marlin F-145B2 CCD (8bits, 1390x1040 pixels, shutter speed 1/125 s and 15fps) and the processing of phase map carried out by IDEA software (Robinson and Reid (1993)).

Optimization algorithm

In this work, the optimization algorithm was based on Visual Basic[®] existing code (Mccaffrey (2015)) and modified for this specific application. Basically it starts with a random value of Young's modulus to find displacements at the same points measured in the experiments. Although the bone should not be considered as an isotropic material, for simplification, it was assumed a homogeneous, linear and isotropic material in order to calculate the analytical displacements by applying the Equation (6).

The inputs for the PSO algorithm were the load, the sample length, the moment of inertia and a separated file containing the position and displacements from the experiments. The numbers of iterations, number of particles and boundaries were also required for optimization. Boundaries were considered the minimum and maximum Young's modulus assigned by the user. It was considered Young's modulus values from the literature that reported a variation between 8 and 22.8 GPa (Bosisio et al. (2007)). Based on those values, the boundaries for the PSO algorithm were established.

The algorithm also compares the two ranges of values (experimental and analytical displacements) in order to provide the difference from both ranges of values. Based on this difference, the algorithm tried a new Young's modulus value in order to minimize

the error to the subsequent iteration. After the total number of iterations achieved, the algorithm stopped the analysis and indicated the estimated Young's modulus for the bone sample (Figure 3).

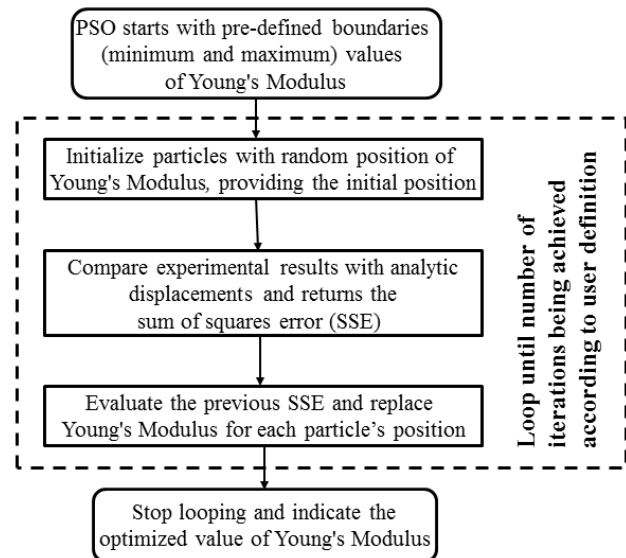


Figure 3: PSO flow chart for Young's modulus determination.

Finite Element Analysis

By knowing the estimated Young's modulus from PSO in conjunction of the scanned bone geometry, numerical simulations were able to be performed. Those data were considered as inputs for the FEA software (ANSYS[®]) and the expected outputs are the simulated displacements.

In order to run the Finite Element analysis, it was necessary to generate the mesh (discretized model) from the bone geometry. This process consists on the geometric model subdivision in small volumes (nodes and elements). In the case of this work, bone mesh generated 266 nodes and 144 elements (hexahedral eight node element with reduced integration). External load were applied to a node in the same position of DSPI experiments.

RESULTS AND DISCUSSION

DSPI measurement results including fringe patterns with phase-shifting and phase maps from the radius bone is shown in Figure 4.

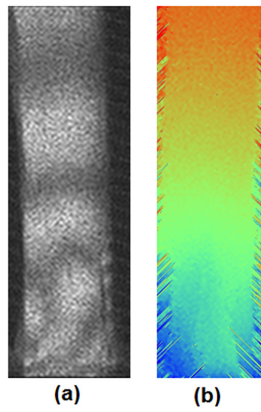


Figure 4: Fringes (a) and phase map (b) from radius bone.

From experimental data, a third order polynomial curve was obtained from DSPI measurements and it was defined as the objective function, according to Equation (9).

$$y = (-3.1 e-9)x^3 + (8.6-7)x^2 + (1.4 e-11)x - 2.5e-10 \quad (9)$$

where x represents the bone length and y is the DSPI displacement measurements.

In order to run the algorithm, a hundred iterations have been chosen since it was enough for the Young’s modulus stabilization as observed in previous algorithm running tests. Ten particles were chosen for the analysis in the algorithm. It means that after ten PSO iteration, it was carried out over just one particle to the next iteration (best position). For this reason, Figure 5 presented the optimization result showing a total of 1000 iterations (10 particles times 100 iterations).

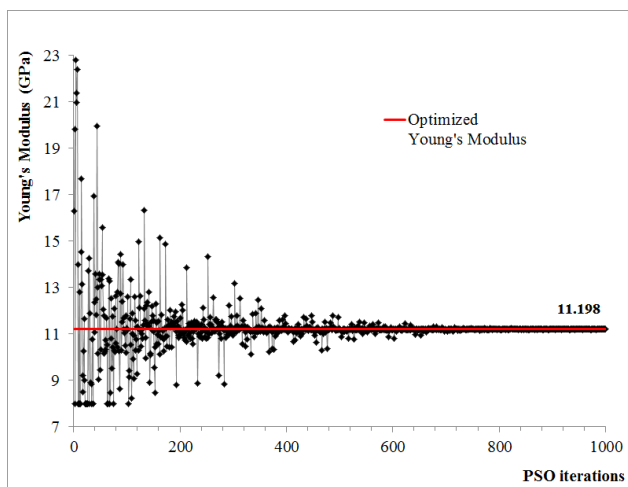


Figure 5: Optimization results for Young’s Modulus estimation.

In Figure 5, it is observed the estimated Young’s modulus value around 11.2 GPa. In order to certify the stability of the optimization method, wide boundary conditions were established (1 to 50 GPa), taking in consideration Young’s modulus values of some less familiar bony tissues (Currey (2010)). It is noted that even changing the input parameter to a wide boundary, the results kept the same which certified the stabilization of the algorithm.

The estimated Young’s modulus obtained from DSPI together with PSO was close to the literature, such as Martinez-Celorio et al. (2010) which reported 12.9 GPa by using interferometry as well. This certified the use of the estimated Young’s modulus (from PSO algorithm) for displacements prediction by means of Finite Element simulations. Figure 6 presents displacements results from FEA based on the Young’s modulus equals to 11.198 GPa.

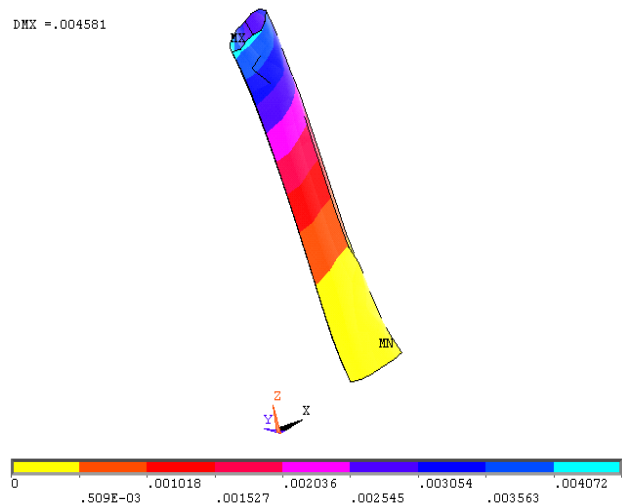


Figure 6: FEA displacements results (mm) from the bone geometry.

Figure 7 presents DSPI results (including standard deviation values) versus FEA displacements considering the simulations with estimated bone Young’s modulus.

Considering the clamping position at zero mm, it is noted in the Figure 5 that from the distance around 70 mm to 92 mm, which is the total length of the bone, the difference between both curves were increased (FEA curve out of DSPI standard deviation values), although the total error was close to 3%. This increasing difference from both curves can be explained by the hypothesis that as higher as the displacements, more sensitive was the DSPI measurements. This can be considered an advantage for optical applications which

require high sensitivity as reported by Braga Jr et al. (2015).

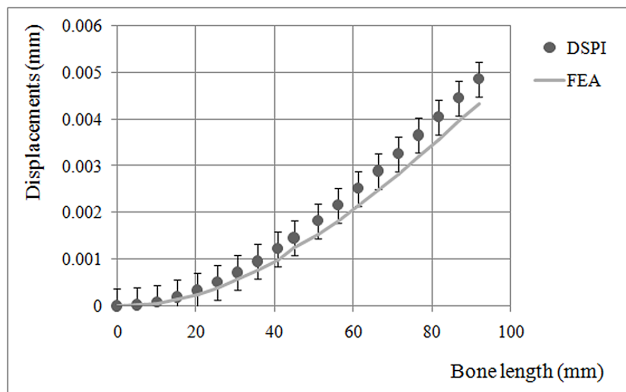


Figure 7: FEA vs. DSPI displacements results with standard deviation.

CONCLUSIONS

In this work, DSPI together with an optimization algorithm for displacements measurements of a bone sample was evaluated by comparing with FEA. Results showed 3% difference between DSPI and FEA displacements data, considering simulations with estimated Young's modulus of 11.198 GPa obtained from the PSO algorithm.

The geometry of the bone model was considered linear only in the PSO algorithm, but in bending tests and finite elements analysis, it is not. PSO algorithm was used for Young's Modulus estimation and comparison results were performed between DSPI and finite elements results.

Results also demonstrated that as higher as the displacements, more sensitive was the DSPI measurements and this can be considered an advantage for optical applications which require high sensitivity. This demonstrates the potentiality of DSPI together with optimization methods for other biomechanics applications.

ACKNOWLEDGEMENTS

This research project was partially supported by CAPES and University of Liverpool.

REFERENCES

ARUMUGAM, M.S.; RAO, M.V.C. Molecular docking with multi-objective Particle Swarm Optimization. *Applied Soft Computing*, 8: 666-675, 2008.

BOSISIO, M.R. et al. Apparent Young's modulus of human radius using inverse finite-element method. *Journal of Biomechanics*, 40: 2022-2028, 2007.

BRAGA JR, R.A. et al. Maps of deformations in a cantilever beam using particle image velocimetry (PIV) and speckle patterns. *Revista Escola de Minas*, 68: 273-278, 2015.

CURREY, J.D. Mechanical properties and adaptations of some less familiar bony tissues. *Journal of the Mechanical Behavior of Biomedical Materials*, 3: 357-372, 2010.

FACCHINI, M.; ZANETTA, P. An ESPI in-plane system applied to the evaluation of mechanical characteristic of masonry. *Measurement Science and Technology*, 6: 1260-1269, 1995.

GONZÁLEZ, R. et al. Measurement of Young's modulus of cementitious materials using an electro-optic holographic technique. *Optics and Laser in Engineering*, 36: 527-535, 2001.

GOODMAN, J.W. Speckle phenomena in optics. Theory and applications. *Robert and Company Publishers*, 2007, 384 p.

HILL, I.; BANKS, S. Serial manipulator functional calibration for in vitro biomechanical testing. *Journal of Biomechanics*, 47: 289-292, 2014.

JIANG, Y. et al. Particle Swarm Optimization based on dynamic niche technology with applications to conceptual design. *Advances in Engineering Software*, 38: 668-676, 2007.

KOH, B. et al. Limitations of parallel global optimization for large-scale human movement problems. *Medical Engineering & Physics*, 31: 515-521, 2009.

KOH, B. et al. Parallel asynchronous Particle Swarm Optimization. *International Journal for Numerical Methods in Engineering*, 67: 578-595, 2006.

LANG, H. et al. Determination of the dynamics of restored teeth by 3D electronic speckle pattern interferometry. *Lasers in Surgery and Medicine*, 34: 300-309, 2004.

LIU, L.; LIU, W.; CARTES, D.A. Particle Swarm Optimization-based Parameter Identification Applied to Permanent Magnet Synchronous Motors. *Engineering Applications of Artificial Intelligence*, 21: 1092-1100, 2008.

- LOJA, M.A.R. On the use of particle swarm optimization to maximize bending stiffness of functionally graded structures. **Journal of Symbolic Computation**, 61-62: 12-30, 2014.
- MAGALHAES, R.R.; BRAGA JR, R.A.; BARBOSA, B.H.G. Young's Modulus evaluation using Particle Image Velocimetry and Finite Element Inverse Analysis. **Optics and Lasers in Engineering**, 70: 33-37, 2015.
- MARTINEZ-CELORIO, R.A. et al. Young's modulus measurement of the radius bone using a shearing interferometer with carrier fringes. **Optics and Lasers in Engineering**, 48: 727-731, 2010.
- MARWALA, T. Finite Element Model Updating Using Particle Swarm Optimization. **International Journal of Engineering Simulation**, 6: 25-30, 2005.
- MAZHOUD, I. et al. Particle swarm optimization for solving engineering problems: A new constraint-handling mechanism. **Engineering Applications of Artificial Intelligence**, 26: 1263-1273, 2013.
- MCCAFFREY, J. Particle Swarm Optimization. Available at: <https://msdn.microsoft.com/magazine/hh335067>. Accessed on: May, 05, 2015.
- PARVITTE, B. et al. Quantitative simulation of photoacoustic signals using finite element modelling software. Applied Physics B: **Lasers and Optics**, 111: 383-389, 2013.
- PETZING, J.N. et al. The analysis of human femur and prostheses using Electronic Speckle Pattern Interferometry. **Engineering Science and Education Journal**, 7: 35-40, 1998.
- REILLY, D.T.; BURSTEIN, A.H.; FRANKEL, V.H. The elastic modulus for bone. **Journal of Biomechanics**, 7: 271-276, 1974.
- ROBINSON, D.W.; REID, G.T. Interferogram analysis: Digital fringe pattern measurement techniques, **Institute of Physics Publishing**, 1993, 302 p.
- ROMÁN, J.F. et al. The mechanical behavior of human mandibles studied by Electronic Speckle Pattern Interferometry. **The European Journal of Orthodontics**, 21: 413-421, 1999.
- SCHUTTE, J.F. Evaluation of a particle swarm algorithm for biomechanical optimization. **Journal of Biomechanical Engineering**, 127: 465-474, 2005.
- SU, M. et al. Measurement of bone strain using electronic Speckle Pattern Interferometry. **Journal of Holography and Speckle**, 2: 34-39, 2005.
- TIMOSHENKO, S.P.; GOODIER, J. N. Theory of Elasticity, **McGraw Hill Book Company**, 1970. 591 p.
- YANG, A. et al. Computation of physiological human vocal fold parameters by mathematical optimization of a biomechanical model. **Journal of the Acoustical Society of America**, 130: 948-964, 2011.